

## PREDICTING THE DYNAMIC STRUCTURAL RESPONSE CONTROLLED BY A SLOSHING ABSORBER USING SPH

Adam MARSH<sup>1</sup>, Mahesh PRAKASH<sup>2\*</sup>, S.E. SEMERCIGIL<sup>1</sup> and Ö. F. TURAN<sup>1</sup>

<sup>1</sup>School of Engineering and Science

Victoria University, Melbourne, Victoria, 3011 AUSTRALIA

<sup>2</sup>CSIRO Mathematical and Information Sciences, Clayton, Victoria 3169, AUSTRALIA

\*Corresponding author, Email address: Mahesh.Prakash@csiro.au

### ABSTRACT

A sloshing absorber consists of a container, partially filled with fluid to possess a free surface. The absorber is attached to the structure to be controlled, and relies on the structure's motion to excite the liquid. Consequently, sloshing waves are produced at the free surface, possessing energy dissipative qualities. The behaviour of liquid sloshing has been well documented in the literature, although its use as a structural control agent has attracted considerably less attention.

The sloshing absorber's ability to control a light resonant structure is demonstrated experimentally. The effect of liquid depth on control performance is analysed. An ideal range is identified. Smoothed Particle Hydrodynamics (SPH) is then used to model the dynamic structure/sloshing absorber system. The objective is to demonstrate the technique's ability to reliably predict fluid-structure interaction forces.

When tuned properly, these interaction forces generate the required control of excessive structural oscillations. A series of shallow liquid levels are investigated to generate travelling free surface waves. Predicted free surface shapes and the resulting structural response are then compared to those observed experimentally. Close correspondence is reported between predictions and experiments, for a wide range of liquid depths.

### INTRODUCTION

Sloshing is the low frequency oscillation of a liquid within a partially full container. In study of sloshing, efforts are usually made in the direction of suppression due to the damaging effects it can impose (Popov et al., 1993; Faltinsen, 1993).

On the other hand, sloshing has an inherent ability to dissipate large amounts of energy via shearing of the fluid. For this reason, it is possible to employ liquid sloshing as an effective energy sink in structural control applications, providing protection for structures exposed to excessive vibration levels (Sun and Fujino, 1994; Modi et al., 1996; Tamura et al., 1996; Modi and Munshi, 1998; Banerji et al., 2000).

A sloshing absorber is simply a container attached on the structure to be controlled as shown in Figure 1. Sloshing in the container is induced intentionally for structural control. The absorber is tuned so that the frequency of sloshing normally coincides with the natural frequency of the structure. The sloshing fluid oscillates out of phase with mass  $m$ , creating a counteracting pressure force on the sides of the container. Shear stress within the fluid is the primary form of mechanical damping in this type of absorber, if the liquid level is low.

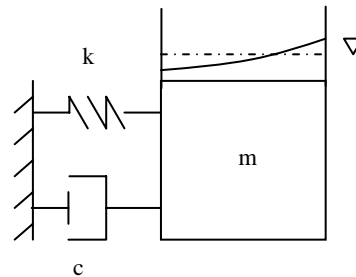


**Figure 1:** Tuned liquid damper, attached to a mechanical oscillator of mass  $m$ , stiffness  $k$  and viscous damping coefficient of  $c$ .

In this paper, simple experiments are described, involving an inverted pendulum controlled by a sloshing absorber. The effect varying the liquid depth within the absorber has on structural control is demonstrated, identifying an ideal depth range. The Smoothed Particle Hydrodynamics (SPH) method is then used to model dynamic behaviour of the structure/sloshing absorber system in two dimensions. The numerical predictions of structure motion and fluid free surface shapes are compared to those observed experimentally. The objective is to demonstrate the modelling technique's ability to accurately predict the physics of such fluid-structure interaction problems.

### THE SPH METHOD

Smoothed Particle Hydrodynamics (SPH) is used in this study, due to its ability to capture complex free surface behaviour accurately. The code used here has been developed by CSIRO's Mathematical and Information Sciences Division. A broad range of complex industrial fluid flow problems have been modelled successfully with this code (Cleary et al., 2007).

SPH is a particle-based method of modelling fluid flows. The fluid being modelled is discretized into fluid elements, the properties of which are attributed to their centres. SPH is a Lagrangian continuum method used for solving systems of partial differential equations. The method works by tracking particles and approximating them as moving interpolation points.

The interpolated value of any particle property  $A$  at position  $r$  is approximated using the information from nearby particles lying within a radius of  $2h$  from the particle of interest, and is governed by Equation 1.

$$A(r) = \sum_b m_b \frac{A_b}{\rho_b} W(r - r_b, h) \quad (1)$$

Where:  $W$  is an interpolation kernel  
 $h$  is the smoothing length  
 $m_b$  is the mass of particle  $b$   
 $r_b$  is the position of particle  $b$   
 $\rho_b$  is the density of particle  $b$   
 $A(r)$  is property  $A$  of a particle at position  $r$

The SPH continuity equation is,

$$\frac{d\rho_a}{dt} = - \sum_b m_b (v_a - v_b) \cdot W_{ab} \quad (2)$$

where  $W_{ab} = W(r_{ab}, h)$  and is evaluated for the distance  $|r_{ab}|$ .  $r_{ab}$  is the position vector from particle 'b' to particle 'a' and is equal to  $r_a - r_b$ .

The SPH momentum equation is,

$$\frac{dv_a}{dt} = - \sum_b m_b \left[ \left( \frac{P_b}{\rho_b^2} + \frac{P_a}{\rho_a^2} \right) - \frac{\zeta}{\rho_a \rho_b} \frac{4\mu_a \mu_b}{(\mu_a + \mu_b)} \frac{v_{ab} r_{ab}}{(r_{ab}^2 + \eta^2)} \right] \nabla_a W_{ab} + g \quad (3)$$

where  $P_a$  and  $\mu_a$  are the pressure and viscosity of particle 'a', the same applies for particle 'b'.  $v_{ab} = v_a - v_b$ , the velocity of particle 'b' subtracted from the velocity of particle 'a'.  $\zeta$  is a factor having a theoretical value of 4.  $\eta$  is a parameter used to smooth out the singularity at  $r_{ab} = 0$ , and  $g$  is the gravitational acceleration.

SPH uses a compressible method for determining the fluid pressure. It is operated near the incompressible limit by selecting a speed of sound that is much larger than the velocity scale expected in the fluid flow.

The equation of states that governs the relationship between particle density and fluid pressure is,

$$P = P_0 \left[ \left( \frac{\rho}{\rho_0} \right)^\gamma - 1 \right] \quad (4)$$

where  $P_0$  is the magnitude of pressure and  $\rho_0$  is the reference density. The pressure the equation of state solves for  $P$  is then used in the SPH momentum equation governing the particle motion. For water,  $\gamma = 7$  is generally used. A more detailed description of the method can be found in Monaghan, 1992.

## EXPERIMENTAL PROCEDURE

The experimental setup shown in Figure 2, consists of a mechanical oscillator whose structure is configured as an inverted pendulum. Structural stiffness is provided by attached springs. A rectangular container to accommodate the sloshing absorber is mounted on the pendulum, 670 mm above the pivot point. Hence, as the structure is excited the container is subject to angular oscillations. The container is 340 mm long (in the direction that waves travel), 230 mm wide and 180 mm high.

The disturbance is provided from an initial angular displacement of 16 degrees (the structure is shown in this position by the dashed lines in Figure 2). A simple stop-block allows consistent initial conditions for all cases. The structure is released from its initial position and allowed to oscillate freely. Experimental observations are video recorded with a standard digital camera at a frame speed of 30 frames per second.

The natural frequency and equivalent viscous damping ratio of the uncontrolled structure are  $0.5 \text{ Hz} \pm 0.02$  and  $0.9 \% \pm 0.1$ , respectively. The sloshing absorber is tuned to this frequency when a depth of  $\sim 12 \text{ mm}$  is employed (Milne-Thomson, 1968). However, this process of tuning is not able to take the effect of free surface discontinuities into account.

The mass moment of inertia of the uncontrolled structure is measured to be approximately  $3.4 \text{ kg.m}^2$  about the centre of rotation. The ratio of mass moment of inertia of fluid to that of the structure for the above-mentioned liquid depths is about 1/34 (2.75 mm), 1/17 (5.5 mm), 1/11 (8.25 mm), 1/9 (11 mm) and 1/4 (22 mm). The ratio of fluid mass to structure mass for these liquid depths is about 1/80 (2.75 mm), 1/40 (5.5 mm), 1/27 (8.25 mm), 1/20 (11 mm) and 1/10 (22 mm).

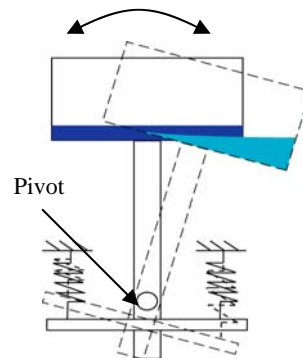


**Figure 2:** Showing the structure and the sloshing absorber at rest (vertical) and at initially displaced positions.

## NUMERICAL MODEL

The structure and sloshing absorber are represented by a single rigid boundary, having the same dimensions as the experimental setup. This boundary is constructed of a single layer of SPH particles. These particles exert a repulsive force, of the Lennard-Jones form, on the fluid particles in their normal direction (Monaghan, 1994). The boundary's motion is restricted to dynamic rotation about its pivot point. Tethers are attached, representing the force relationship between the structure and supporting springs. This relationship exists due to the system's stiffness and viscous damping properties.

The sloshing fluid is water with a density of  $1000 \text{ kg.m}^{-3}$  and dynamic viscosity of  $0.001 \text{ Pa.s}$ . A particle size of  $0.5 \text{ mm} \times 0.5 \text{ mm}$  has been found to be fine enough to model the boundary and water within. A resolution study has been completed (Marsh, 2009), but is not shown here for brevity. Time stepping is explicit and is limited by the Courant condition modified for the presence of viscosity (Monaghan, 1992).

To replicate the experimental conditions, the structure/absorber system is given an initial displacement of  $16^\circ$  clockwise, storing potential energy in the tethers. The fluid is allowed to settle for 4 seconds in this position until the liquid velocity approaches  $0 \text{ m/s}$ . The structure is then released responding dynamically, its motion excites the liquid within. Structure motion ceases due to the damping of the attached tethers, and the additional control of the working fluid.

## LIQUID SLOSHING AND STRUCTURAL RESPONSE

### Free Surface Comparison

Free surface comparisons at a liquid depth of  $5.5 \text{ mm}$  are shown in Figure 3, to illustrate the ability of SPH to capture the fluid behaviour. The left hand column represents experimental observations at certain instants in time, numerical predictions are shown in the right hand column. Figures 3(a) and (b), (c) and (d), (e) and (f), (g) and (h), (i) and (j), and (k) and (l) correspond to times of  $0.93 \text{ s}$ ,  $1.13 \text{ s}$ ,  $2.20 \text{ s}$ ,  $2.34 \text{ s}$ ,  $2.74 \text{ s}$ , and  $5.44 \text{ s}$  respectively from the instant of release. These nominated instances are chosen either as points of reference (when the structure is in the central rest position, or at maximum rotation), or at points in time where fluid behaviour is exceptionally interesting.

At the instant of its release, structure motion commences from right to left. At  $t = 0.93 \text{ s}$ , the travelling wavefront shown in Figure 3(a) impacts on the left wall, causing a wave-to-wall interaction. The predicted wavefront reaches the container wall prior to this instant, resulting in a small phase difference between experimental and numerical fluid flow of  $\sim 0.02 \text{ s}$ .

High wavefront velocity causes a hydraulic jump with a maximum height recorded at  $t = 1.13 \text{ s}$ . Significant swirling behaviour is seen in Figure 3(c) at this instant. Hydraulic jump behaviour is predicted well, however the initial phase difference between the experimental and numerical fluids is noticeable still in Figure 3(d).

The wave to wall interaction that follows, at the right side of the container, is shown in Figure 3(e). Peak rotation is also observed at this instant. Fluid distribution is predicted well in Figure 3(f). However, the predicted hydraulic jump height is marginally smaller than that observed.

The swirling, elevated fluid then falls under gravity, impacting on the container bottom at  $t = 2.34 \text{ s}$ . Severe mixing is observed at this instant as a result, shown in Figure 3(g). Although the details of this behaviour cannot be captured, possibly due to the lack of a turbulence model, fluid distribution is predicted well.

The structure passes through the central rest position shortly after at  $t = 2.74 \text{ s}$ . Fluid is distributed over three quarters of the container bottom at this instant, shown in Figure 3(i). The predicted fluid free surface length is smaller than that observed. The phase difference between the experimental and numerical fluids has reduced.

Wave-to-wall interaction during the third cycle of structural oscillation is shown in Figure 3(k). Maximum anti-clockwise rotation is achieved at this instant. Fluid behaviour is less energetic here than during the previous wave to wall interactions. Fluid distribution and wave to wall interaction behaviour are predicted well.

At the depth of  $5.5 \text{ mm}$ , SPH provides a close representation of the fluid free surface behaviour within the absorber. Some observed local fluid behaviour is not replicated exactly, particularly during energetic hydraulic jumps. During such events, it is not uncommon to observe significant swirling of the fluid. Overall fluid distribution is accurately predicted at all instances. This overall behaviour seems to be more important than local detail, due to the pressure force exerted on the structure by the fluid being an integral quantity. As a result, the structure's motion is relatively insensitive to the small scale details of the free surface.

### Settling Times

A summary of experimental settling times for the structure controlled by the sloshing absorber with varying liquid depth is shown in Figure 4(a). Here, settling time is defined as the time taken from the structure's release to when its motion has ceased, residing in the central rest position. Cases employing all levels of liquid studied here produce a considerable reduction in settling time, relative to the uncontrolled case (liquid depth of zero).

Settling time is shortest (about  $12 \text{ s}$ ) when employing a liquid depth of either  $5.5 \text{ mm}$  or  $8.25 \text{ mm}$ . In fact, settling time is largely insensitive to the amount of fluid within the absorber between depths of  $2.75 \text{ mm}$  and  $11 \text{ mm}$ . At all these depths, the travelling waveform is dominant. At  $22 \text{ mm}$  of depth, standing waves are observed. As a result, settling time increases significantly.

Optimum performance of the sloshing absorber occurs at a depth shallower than that of the tuned case ( $\sim 12 \text{ mm}$ ). At these shallow depths, there are extreme discontinuities in the flow field. Steep velocity gradients occur as a result, producing large amounts of shear stress and inherent energy dissipation. Therefore, it seems more important to select a liquid depth that maximises energy dissipation, as

opposed to one that tunes the sloshing frequency to that of structure's frequency.

A comparison of settling times between the SPH predictions and experimental data is shown in Figures 4(b) to 4(f) for liquid depths of 2.75 mm, 5.5 mm, 8.25 mm, 11 mm and 22 mm respectively. Here, settling time is defined as the time taken from the instant of the structure's release to when it reaches a certain percentage of its initial rotation. This percentage is indicated on the horizontal axis in these figures. The vertical axis represents settling time in s. The error in experimental measurement is expected to be around 1 s and is indicated in the figure with error bars. It can be seen that SPH provides an accurate estimate of settling time for all liquid depths, at all levels of residual displacement.

### Displacement History

The observed angular displacement history of the structure is compared to the SPH prediction of the uncontrolled case, along with the 2.75 mm, 5.5 mm, 8.25 mm, 11 mm, and 22 mm liquid depth cases. These are shown in Figures 5(a) to 5(f). In the figures the horizontal axis is normalised time by the period of oscillation ( $T_n$ ).

The SPH prediction of the uncontrolled structure's motion is an exact match to that seen experimentally. The quality of prediction when the structure is controlled varies with liquid depth. However, a good representation is obtained when fluid behaviour is 'dynamic'. These instances are typically seen when the structure is experiencing large displacements and for shallow liquid levels. For depths of 2.75 mm and 5.5 mm, dynamic behaviour is observed almost all the time. As liquid depth increases, dynamic fluid behaviour is observed less often.

Whilst fluid behaviour is dynamic, predicted peak amplitudes and the frequency of structural oscillation are close to those observed experimentally. As structure displacements become small (less than about  $6^\circ$ ), the fluid behaviour becomes less dynamic. At these instances, more energy dissipation seems to be predicted than observed experimentally. As a result, predicted peak displacements are smaller than those observed for all liquid depths.

At the depths of 8.25 mm and higher, enough excess energy dissipation is predicted to affect the structure's damped frequency ( $\omega_d$ ), as per the relationship in equation 5.

$$\omega_d = \omega_n \sqrt{1 - \zeta_{eq}^2} \quad (5)$$

Where  $\omega_n$  is the undamped natural frequency of the structure, and  $\zeta_{eq}$  is the structural damping caused by energy dissipation within the fluid.

Excessive  $\zeta_{eq}$  causes reduction in structure frequency, resulting in the developing phase observed in Figures 5(d), 5(e) and 5(f). The authors are currently working to correct this problem. However, even with this difficulty, SPH provides a good representation of the structure's behaviour when controlled by all liquid depths.

### CONCLUSION

A sloshing absorber can successfully mitigate vibration of a light resonant structure. To optimise control, it is more important to select a liquid depth that maximises energy dissipation, than one that tunes the sloshing frequency to coincide with the natural frequency of the structure. The sloshing absorber's performance in terms of settling time is largely insensitive to the amount of fluid used, within a range of liquid depths. Such insensitivity is of great practical advantage from a design point of view.

SPH has been used to predict the fluid-structure interaction between a structure and the sloshing absorber. The quality of prediction appears to be dependent on the nature of fluid behaviour, being more accurate when the flow is dynamic. When the fluid is relatively less dynamic, excess energy dissipation appears to be predicted. This results in the forecasting of lower peak displacements for the structure than those observed. In liquid depths of 8.25 mm and higher, the predicted period of structural oscillation increases during small displacements, also seemingly as a result of excessive energy dissipation within the fluid. This problem is currently being investigated.

At the liquid depth of 5.5 mm, free surface shapes are predicted well. Some observed local fluid behaviour is not replicated exactly, particularly when hydraulic jumps are observed. Overall fluid distribution is accurately predicted at all instances. This is considered to be more important due to the pressure force exerted on the structure by the fluid being an integral effect. Overall, SPH predicts the behaviour of the structure/sloshing absorber system soundly. At all liquid depths SPH provides a good prediction of settling time and structure motion, proving the method to be a valuable tool for sloshing absorber design.

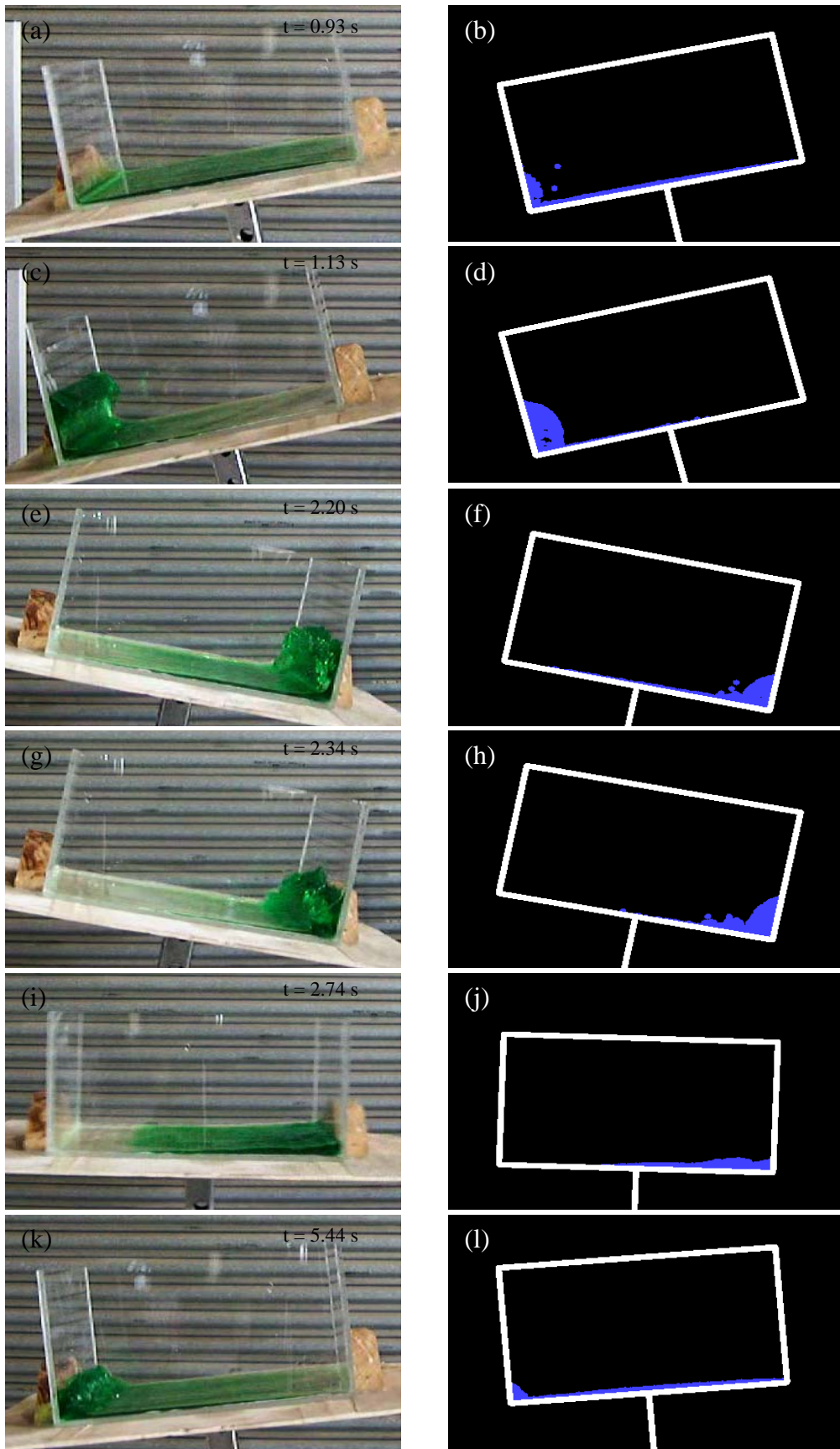


**Figure 3:** Free surface comparisons of 5.5 mm liquid depth at different marked instances. Left column has the experimental observations and right column has the numerical predictions.

## REFERENCES

BANERJI, P., MURUDI, M., SHAH, A.H., POPPELWELL, N., (2000), "Tuned liquid dampers for controlling earthquake response of structures", *Earthquake Engineering and Structural Dynamics*, **29**, 587-602.

CLEARY, P.W., PRAKASH, M., HA, J., STOKES, N., SCOTT, C., (2007), "Smooth Particle Hydrodynamics: status and future potential", *Progress in Computational Fluid Dynamics*, **7**, 70-90.

FALTINSEN, O. M., (1993), "Sea Loads on Ships and Offshore Structures", *Cambridge University Press*, Cambridge.

MARSH, A.P., (2009), "Design of Effective Travelling-Wave Sloshing Absorbers for Structural Control", *PhD Thesis, Victoria University, Australia*. In preparation.

MODI, V.J., WELT, F., SETO, M.L. (1996), "Control of Wind Induced Instabilities Through Application of Nutation Dampers: a brief overview", *Journal of Engineering and Structures*, **17**, 626-638.

MODI, V.J., MUNSHI, S.R., (1998), "An Efficient Liquid Sloshing Damper for Structural Control", *Journal of Fluids and Structures*, **12**, 1055-1071.

MONAGHAN, J.J., (1992). "Smoothed particle hydrodynamics", *Ann. Rev. Astron. Astrophys.*, **30**, 543-574.

MONAGHAN, J.J., (1994). "Simulating Free Surface Flows in SPH", *Journal of Computational Physics.*, **110**, 399-406.

POPOV, G., SANKAR, S., SANKAR, T. S., (1993), "Dynamics of Liquid Sloshing in Baffled and Compartmented Road Containers", *Journal of Fluids and Structures*. **7**, 803-821.

SUN, L.M., FUJINO, Y., (1994), "A Semi-Analytical Model for Tuned Liquid Damper (TLD) with Wave Breaking", *Journal of Fluids and Structures*, **8**, 471-488.

TAMURA, Y., KOHSAKA, R., NAKAMURA, O., MIYASHITA, K., MODI, V.J., (1996), "Wind-Induced Responses of an Airport Tower – efficiency of a tuned liquid damper", *Journal of Wind Engineering*, **65**, 121-131.

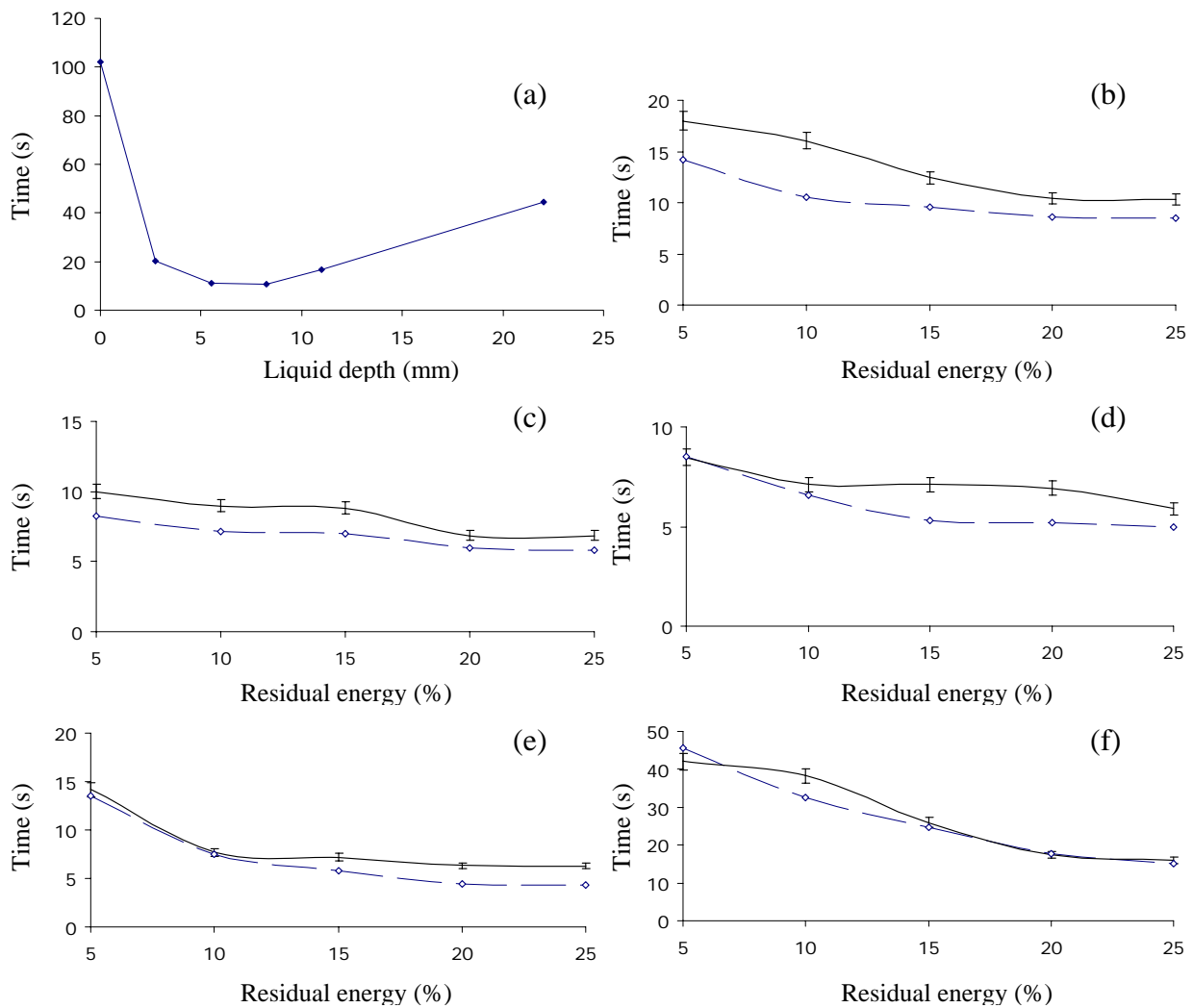


**Figure 4:** (a) Variation of experimentally observed settling time with liquid depths and comparisons for (b) 2.75 mm, (c) 5.5 mm, (d) 8.25 mm, (e) 11 mm and (f) 22 mm liquid depths between experiments (—) and predictions (---).

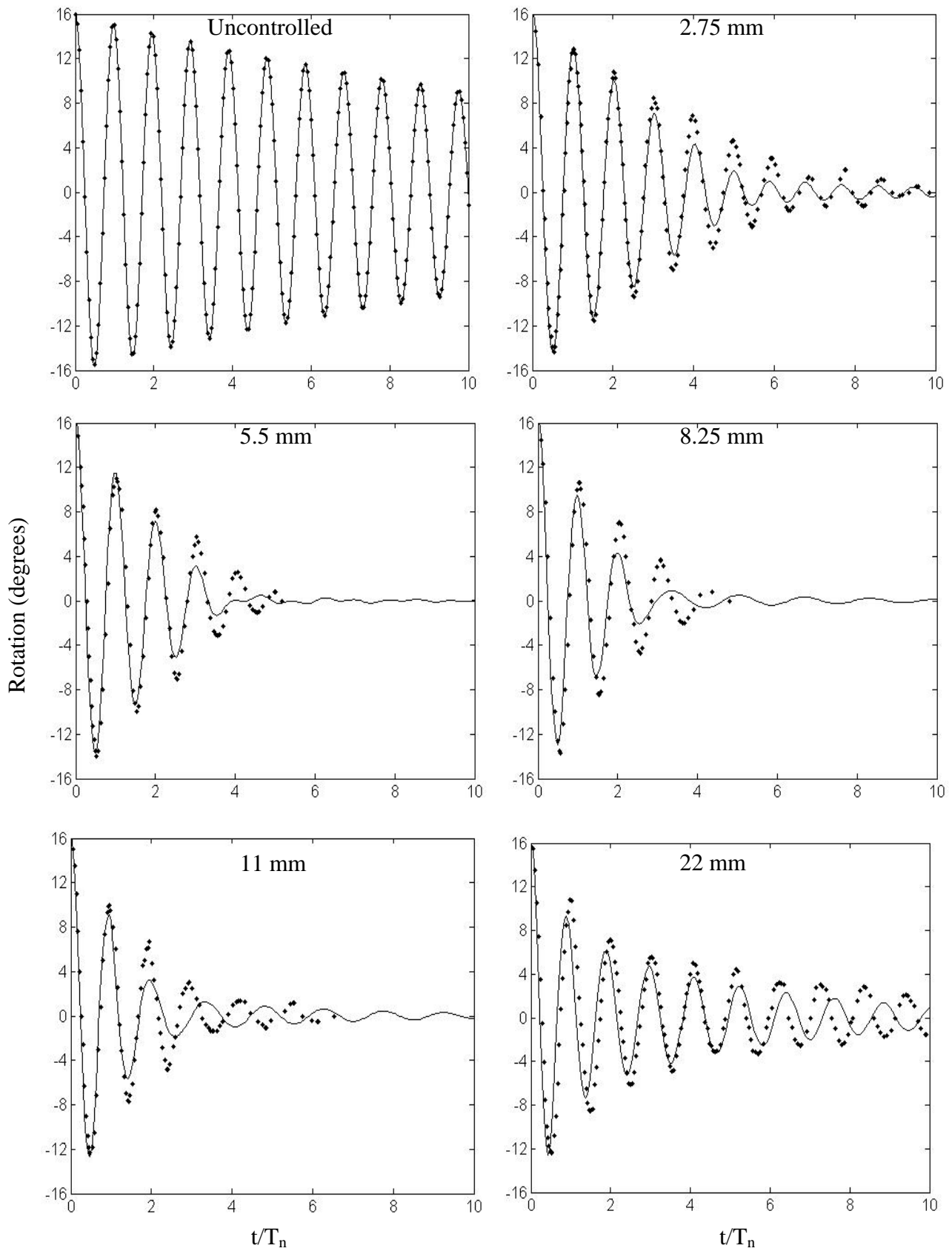


**Figure 5:** History of angular displacement of experimental observations (●) and SPH predictions (—) for (a) uncontrolled, (b) 2.75 mm, (c) 5.5 mm, (d) 8.25 mm, (e) 11 mm and (f) 22 mm deep cases.